PHYSICAL REVIEW B VOLUME 10, NUMBER 12 15 DECEMBER 1974

Surface molecules and chemisorption. II. Photoemission angular distributions

J. W. Gadzuk
National Bureau of Standards, Washington, D. C. 20234
(Received 18 March 1974)

A theory of the angular distributions of electrons photoemitted from submonolayer films of chemisorbed atoms is presented. Chemisorption is treated within the surface-molecule limit of the Anderson model. It is shown that the key features which differentiate between solid-state photoemission and atomic photoionization are the localization of the hole left behind in the photoexcitation process and the preferential orientation of atomic or molecular orbitals (in photoemission from solids or chemisorbed atoms). The differential photoionization cross sections or angular distributions for spatially oriented atoms and surface molecules are obtained and contours of constant emission intensity, as projected on a flat fluorescent screen which is parallel to the surface, are presented. It is shown that the chemisorption bonding geometry can be ascertained from such measurements.

I. INTRODUCTION

Ultraviolet photoemission studies have become very useful in determining the electronic structure of atoms chemisorbed on metal surfaces.[1-6] The importance of the angular distribution (AD) of photoemitted electrons from clean surfaces has been noted theoretically.[7] Such angular effects have subsequently been observed experimentally[5,8-10] although the full implication of these effects has yet to be understood. It has also been suggested[11] that angular dependences in the electrons which are photoemitted from chemisorbed atoms[12-17] could also provide additional useful information pertaining to chemisorption. In some cases, the AD would be related to the AD of electrons which are photoionized from gas-phase atoms[18-20] or molecules,[21(a)] although certain fundamental modifications to the gas-phase theories would be required. It has recently been realized[11] that one of the major distinctions between gas-phase and chemisorption photoionization results from the fact that in the gas phase the orientation of the atoms is random, thus resulting in differential photoionization cross sections with the simple form $d\sigma/d\Omega = a + b\cos^2\theta$, where θ is the angle between the ejected electron momentum and some photon variable, either polarization or momentum, depending upon the polarization state of the photon.[13] The only atomic-physics information obtainable is indirectly through the value of the ratio b/a. On the other hand, for an atom chemisorbed on a surface, the orientation of the atom is not random, a much more complicated expression for the differential cross section or AD is obtained, and much more information is contained in the resultant AD. In particular, by observing the AD from the molecular orbitals involved in the chemical bond, it is possible, in a relatively simple manner, to ascertain whether the atom is in a fourfold symmetric, bridge, or head-on bonding site. This information is crucial to a quantitative understanding of chemisorption. The remainder of this paper will be devoted to the theory of photoemission AD's from chemisorbed atoms. Attention will be directed towards the angular variations caused by the angular dependence of the initial-state wave function. Since completion of this manuscript, Liebsch[21(b)] has presented a theory of photoemission AD's in which the emphasis is on the angular effects due to the final-state wave function, which in essence is a superposition of plane waves in the vacuum, matched onto Bloch functions in the solid. The angular effects he obtains could be of comparable magnitude with those described in this paper.[21(c)] Thus a complete theory must properly treat both the initial and final states on an equal footing.

The structure of the paper is the following. The necessary background chemisorption theory is presented in Sec. II. The general theory of photoemission from chemisorbed atoms is dealt with in Sec. III. Section IV relates the chemisorption theory, in the surface-molecule limit, to the theory of photoemission AD's. The numerical results and interpretive discussion are given in Sec. V. Final conclusions appear in Sec. VI. The relationship between the gas-phase and solid-state photoejection AD is discussed in Appendix A.

II. CHEMISORPTION THEORY

A general method (based upon a self-consistent-field molecular-orbital theory) for describing the electronic properties of a transition-metal surface with a chemisorbed layer of atoms has been the subject of paper I in this series.[16] The basic idea within the surface-molecule approach is that an adatom with a valence-electron level ϵ_a (appropriately modified to include magnetic effects if necessary[12-14,16,22]) forms a chemical bond with the directed d orbitals on the nearest-neighbor substrate atoms. Owing to band effects in the solid, the d-orbital "eigenvalue" is replaced by the density of

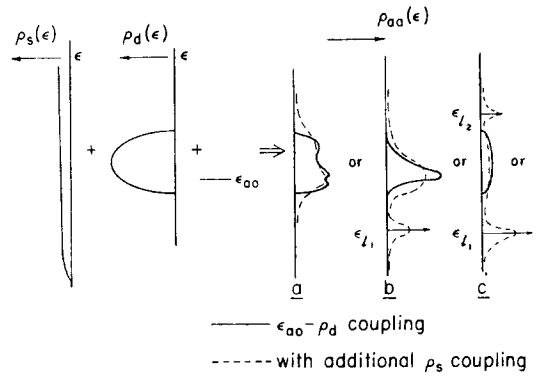

FIG. 1. Relevant densities of states in chemisorption on transition metals. On the left are shown the uncoupled metal s- and d-band densities of states $\rho_s(\epsilon)$ and $\rho_d(\epsilon)$ and also the adatom valence level ϵ_a. On the right in (a), (b), and (c) are shown three possible surface-molecule density of states. The full curve results from the coupling of ϵ_a and $\rho_d(\epsilon)$. The dashed curve results from turning on the coupling with $\rho_s(\epsilon)$.

states $\rho_d(\epsilon)$ as shown in Fig. 1. The coupling between the adatom and metal is represented by the matrix element

$$V_{a\vec{k}} = \langle a | H | \vec{k} \rangle, \tag{1}$$

in which $|a\rangle$ is the discrete valence state of the adatom, $|\vec{k}\rangle$ is an eigenstate of the substrate with $\vec{k}$ vector $(\vec{k}_t, |k_z|)$ and energy $\epsilon(\vec{k})$, z is normal to the surface, and H is the full Hamiltonian of the combined system.

It has been demonstrated[12-14,16,22] that the electronic properties of such a chemisorbed atom can be obtained from the adatom Green's function

$$G_{aa}(\epsilon) = [\epsilon - \epsilon_a - \Lambda(\epsilon) + i\,\Delta_a(\epsilon)]^{-1}, \tag{2a}$$

where

$$\Delta_a(\epsilon) = \pi \sum_{\vec{k}} |V_{a\vec{k}}|^2\, \delta(\epsilon - \epsilon(\vec{k})), \tag{2b}$$

$$\Lambda(\epsilon) = \frac{P}{\pi} \int_{-\infty}^{+\infty} \frac{\Delta_a(\epsilon')}{\epsilon - \epsilon'}\, d\epsilon' , \tag{2c}$$

and P denotes a principal-part integral. The density of states per spin at the adatom is given by

$$\rho_{aa}(\epsilon) = -(1/\pi)\, \mathrm{Im}\, G_{aa}(\epsilon). \tag{3}$$

The energy of the adatom-metal level is given by the "poles" of the adatom Green's function, Eq. (2a),

$$\epsilon - \epsilon_a - \Lambda(\epsilon) = 0. \tag{4}$$

If this value of ϵ falls within the substrate d band, then there are some $\epsilon(\vec{k}) = \epsilon$. Consequently, from Eq. (2b), $\Delta_a(\epsilon)$ is nonzero, in which case the adatom level can be thought of as a resonance or virtual state rather than a true eigenstate. The resulting density of states, from Eqs. (2a) and (3), is

$$\rho_{aa}(\epsilon) = \frac{1}{\pi} \frac{\Delta_a(\epsilon)}{[\epsilon - \epsilon_a - \Lambda(\epsilon)]^2 + \Delta_a^2(\epsilon)}. \tag{5}$$

Three examples of such a density of states are shown as the solid curves in Figs. 1(a)–1(c). In Fig. 1(a), the spectral weight is distributed fairly uniformly throughout the band, whereas in Fig. 1(b), the virtual state displays a peak or resonance within the band.

It is also possible for truly localized states to form if ϵ given by Eq. (4) falls outside the band. When this occurs, the density of localized states is given by

$$\rho_{aa\,l}(\epsilon) = \langle n_a \rangle_l\, \delta(\epsilon - \epsilon_l), \tag{6a}$$

and from Eqs. (2a) and (3)

$$\langle n_a \rangle_l = \left(1 - \frac{\partial \Lambda(\epsilon)}{\partial \epsilon} \bigg|_{\epsilon = \epsilon_l = \epsilon_a + \Lambda(\epsilon_l)} \right)^{-1}, \tag{6b}$$

with subscript l denoting localized. Examples of adatom densities of states in which localized states are removed from the band are shown in Figs. 1(b) and 1(c). In these cases the spectral weight is divided between one or two localized states plus a distributed virtual state. The particular form of $\rho_{aa}(\epsilon)$, for a given system, is determined by factors such as the position of ϵ_a relative to the d band, the strength and k dependence of $V_{a\vec{k}}$, and the substrate band structure. The thrust of this paper will be directed towards a theory of the photoemission AD from surface-molecule states which are split off from the d band. Complicated interference effects between adatom and substrate emission occur when the photoemitted electrons originate from the virtual states, and at present the theory of bulk photoemission is not sufficiently developed to handle this situation.

III. PHOTOEMISSION THEORY

In a photoemission experiment, photons with energy $h\nu$, vector potential $\vec{A}$, and angle of incidence θ_i are directed towards the adsorbate-covered surface. Electrons which occupy the surface molecular levels are excited by the photon into final states $|f\rangle$ with energy $\epsilon_f = \hbar^2 p^2/2m$ and wave vector $\vec{p}$ in the vacuum half-space.

Intuitively from the Golden Rule or formally from Penn,[23] the photoemission energy distribution from a split-off surface-molecule state of the type discussed in Sec. II is

$$\frac{dj_a(\epsilon)}{d\epsilon} = \frac{2\pi e}{\hbar} \sum_f \delta(\epsilon - \epsilon_f) \frac{1}{\pi} \mathrm{Im}\, G_{aa}(\epsilon - h\nu)\, |\langle f | \tau | a_l \rangle|^2, \tag{7a}$$

with

$$\tau = \frac{e}{mc} \vec{A} \cdot \vec{P}_{op} \tag{7b}$$

and

$$|a_l\rangle = |a\rangle + \sum_{\vec{k}} \frac{V_{a\vec{k}}|\vec{k}\rangle}{\epsilon - \epsilon(\vec{k}) - h\nu} \cdot \tag{7c}$$

The sum on f is over all final states which conserve energy and satisfy the relevant optical selection rules which follow from the calculation of the matrix element. This point is discussed at more length in Appendix A. Following Schaich and Ashcroft,[24] the sum on final states in Eq. (7a) is replaced by the integration

$$\sum_f \to \int \frac{d^3p}{(2\pi)^3} \to \frac{m}{\hbar^2(2\pi)^3} \; p\, d\epsilon_f\, d\Omega, \tag{8}$$

where $d\Omega$ is the differential solid angle of the ejected electron. Substituting Eq. (8) into Eq. (7a) and integrating on ϵ_f, the AD from the surface molecule is

$$\frac{dj_a}{d\Omega} = \frac{em}{\hbar^3(2\pi)^2} \int d\epsilon \left(\frac{2m}{\hbar^2}\epsilon\right)^{1/2} \frac{1}{\pi} \mathrm{Im}\, G_{aa}(\epsilon - h\nu) |\langle f|\tau|a_l\rangle|^2. \tag{9}$$

The adatom density of states from Eq. (6a) is

$$(1/\pi)\,\mathrm{Im}\, G_{aa}(\epsilon - h\nu) = \langle n_a\rangle_l\, \delta(\epsilon - h\nu - \epsilon_l),$$

with ϵ_l the discrete value of the localized state. Consequently,

$$\frac{dj_a}{d\Omega} = c\,|\langle f|\tau|a_l\rangle|^2, \tag{10}$$

where now

$$c = \frac{em}{\hbar^3(2\pi)^2}\left(\frac{2m}{\hbar^2}(h\nu + \epsilon_l)\right)^{1/2} \langle n_a\rangle_l$$

and

$$|a_l\rangle = |a\rangle + \sum_{\vec{k}} \frac{V_{a\vec{k}}|\vec{k}\rangle}{\epsilon_l - \epsilon(\vec{k})} \cdot$$

Since in real systems, weak coupling of the surface molecular levels to the s-band continuum broadens the molecular levels,[16,25] as depicted by the dashed curves in Fig. 1, it would be more appropriate to take the split-off density of states as

$$\frac{1}{\pi}\mathrm{Im}\, G_{aa}(\epsilon - h\nu) = \frac{\langle n_a\rangle_l}{\pi} \frac{\Delta_s}{(\epsilon - h\nu - \epsilon_l)^2 + \Delta_s^2},$$

where Δ_s is the natural width due to decay into the s band. Typically $\Delta_s \lesssim 0.5$ eV. It is easily shown that the optical matrix element varies slowly with energy over the width of the broadened level, so it can be removed from the integral of Eq. (9). The resulting AD has exactly the same form as Eq. (10) but now the value of c is slightly different. This is of no importance here, however.

Equation (10) is similar to the gas-phase differential photoionization cross section with one important distinction. In the gas phase, the orientation of the atomic orbitals is random and thus the relevant cross section is obtained by averaging over all azimuthal quantum numbers m. Under these circumstances, the apparent initial state is spherically symmetric and as a result the cross section varies as $a + b\cos^2\theta$, with θ defined previously. The situation in the surface molecule is different since the directions of $|a\rangle$, $|\vec{k}\rangle$, $\vec{A}$, and $\vec{p}$ are defined with respect to a fixed coordinate system determined by the surface geometry. It is for this reason that a careful experimental study of photoemission AD's can provide new information on chemisorption geometry.

IV. OPTICAL MATRIX ELEMENTS

In order to obtain analytic and numerical results for the AD, Eq. (10), the initial state $|a_l\rangle$ must be simplified. According to the surface-molecule approach to chemisorption, the adatom orbital overlaps directional orbitals on the nearest-neighbor substrate atoms to form chemisorption bonds. A number of possible hydrogen bond configurations are shown in Fig. 2. It is then assumed that the dominant coupling between the adatom and metal is through a metal group orbital,[12-17]

$$|g\rangle = (N_g)^{-1/2} \sum_i a_i\, |\varphi_g(\vec{R}_i)\rangle, \tag{11}$$

with $a_i = \pm 1$ depending upon the adsorption site and orbital symmetry, N_g the number of centers in the group orbital, $\vec{R}_i$ the location of the ith atom, and φ_g the substrate orbital of g symmetry ($g = xy, xz, yz, x^2 - y^2, 3z^2 - r^2$ for d bands). Under these circumstances, the atom-metal coupling, Eq. (1), is approximately[16]

$$V_{a\vec{k}} \simeq \langle a|H|g\rangle\langle g|\vec{k}\rangle. \tag{12}$$

It is convenient to express the metal wave functions in the tight-binding form

$$|\vec{k}\rangle = (2/N)^{1/2} \sum_j e^{i\vec{k}_T\cdot\vec{R}_j} \sin(k_z R_{jz} + \delta)\, |\varphi_g(\vec{r} - \vec{R}_j)\rangle, \tag{13}$$

where N is the number of atoms in the crystal,

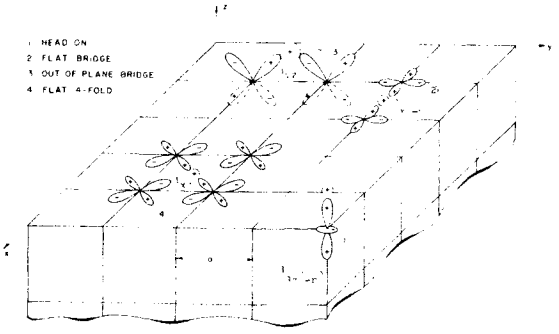

FIG. 2. Some possible chemisorption geometries for an adatom with an s valence level and a d-band substrate.

$\vec{k}_T(k_z)$ is the transverse (normal) component of the wave vector, R_{jz} is the z coordinate of the substrate ion cores in the ith layer, and δ is the phase shift required to satisfy some imposed surface boundary condition.[26] Details and further discussion of this model have been given in I.

It can readily be shown that Eqs. (11)–(13) lead to an initial-state wave function of the form

$$|a_i\rangle = |a\rangle + \sum_i a_i \left(\frac{\beta_g}{\epsilon_i - \bar{\epsilon}}\right) |\varphi_g(\vec{R}_i)\rangle, \tag{14}$$

where the specific value of $\bar{\epsilon}$ depends on the details of the band structure but whose value falls within the band and $\beta_g \equiv (1/N_g)\sum_j a_j \langle \varphi_g(\vec{R}_j)|H|a\rangle$.

In order to calculate the optical excitation matrix element for Eq. (10), an appropriate final state must be chosen. For simplicity and ease in illustrating the role of initial-state symmetries, a plane wave has been chosen, bearing in mind that the complete theory should include the effects discussed by Liebsch.[21(b)] Owing to screening and hole delocalization,[27,28] final-state interactions[29] between the electron and hole should be small and short range, thus obviating the need for Coulomb waves.

To be specific, consider photoexcitation from φ_g on any site $\vec{R}_i$ defined with respect to a coordinate system with origin at the adatom center. The real-space matrix element becomes

$$\langle f|\tau|\varphi_g(\vec{R}_i)\rangle = \frac{\hbar}{i}\frac{e}{mc}\vec{A}\cdot\int d^3r\, e^{-i\vec{p}\cdot\vec{r}}\nabla_{\vec{r}}\varphi_g(\vec{r}-\vec{R}_i). \tag{15}$$

Transforming coordinates $\vec{r}-\vec{r}'+\vec{R}_i$ and letting $\nabla_{\vec{r}'}$ operate on the final state (because of its Hermitian character), Eq. (15) becomes

$$\langle f|\tau|\varphi_g(\vec{R}_i)\rangle = (\hbar e/mc)(\vec{A}\cdot\vec{p})e^{-i\vec{p}\cdot\vec{R}_i}\varphi_g(\vec{p}), \tag{16}$$

with $\varphi_g(\vec{p})$ the Fourier transform of the initial-state wave function. The transform must be performed in a way which preserves the nonrandom orientation of $\varphi_g(\vec{r})$. Podolsky and Pauling[30] were the first to show that if an oriented atomic wave function is of the form $\varphi(\vec{r}) = R_{nl}(r)\sum_m c_m Y_{l,m}(\theta_{\vec{r}}, \varphi_{\vec{r}})$ then

$$\varphi(\vec{p}) = f_{n,l}(p)\sum_m c_m Y_{l,m}(\theta_{\vec{p}}, \varphi_{\vec{p}}), \tag{17}$$

where c_m is a coefficient depending upon the orbital orientation, $f_{n,l}(p)$ is a complicated function discussed in Appendix B, $\theta_{\vec{r}}$, $\varphi_{\vec{r}}$ are the polar angles of $\vec{r}$ in the established coordinate system, and $\theta_{\vec{p}}$, $\varphi_{\vec{p}}$ are the polar angles of the ejected-electron momentum vectors $\vec{p}$ in the same coordinate system.

Combining Eqs. (10), (14), and (17), the complete AD from the surface molecule is given by

$$\frac{dj_a}{d\Omega} \sim \cos^2\gamma \left|\varphi_a(\vec{p}) + \frac{N_g\beta_g}{\epsilon_i - \bar{\epsilon}}\varphi_g(\vec{p})\sum_i \frac{a_i}{N_g}e^{-i\vec{p}\cdot\vec{R}_i}\right|^2, \tag{18}$$

with $\gamma = \sphericalangle\,\vec{p},\vec{A}$, $\cos\gamma = \cos\theta_{\vec{p}}\cos\theta_{\vec{\epsilon}} + \sin\theta_{\vec{p}}\sin\theta_{\vec{\epsilon}}\cos(\varphi_{\vec{p}} - \varphi_{\vec{\epsilon}})$, and $\theta_{\vec{\epsilon}}$ and $\varphi_{\vec{\epsilon}}$ the polar angles of the photon polarization vectors. The expressions for $\varphi(\vec{p})$ must be obtained according to the prescription given by Eq. (17). Specification of the bond geometry is required to evaluate the sum on lattice sites. The effects of preferential orientation appear in several ways in Eq. (18). The particular angular dependences in $\varphi_a(\vec{p})$ and $\varphi_g(\vec{p})$ are defined by the bond geometry as is the bond-site structure factor:

$$S(a,g;\vec{p}) \equiv \sum_i \frac{a_i}{N_g}e^{-i\vec{p}\cdot\vec{R}_i}, \tag{19}$$

where the indices a and g label the adatom angular quantum numbers and group orbital symmetry, respectively.

In Sec. V, three specific chemisorption systems will be considered. First an adsorbate with an oriented p valence level in the limit in which $N_g\beta_g/(\epsilon_i - \bar{\epsilon}) - 0$ will be discussed. Under these conditions the substrate emission is negligible and thus the question of substrate properties need not be raised. Next an s adsorbate on the (100) face of a d-band metal is investigated since this represents H adsorption on a transition metal. Lastly, the more complicated case of a p adsorbate on a d-band metal will be studied since this could be the model for O or C on transition metals.

V. RESULTS

A. Oriented p orbitals

The simplest illustration of the power of AD measurements occurs when the adatom emission, at a given energy ϵ_i, is much larger than the substrate emission. Under these circumstances, the second term in Eq. (18) can be neglected, and Eqs. (17) and (18) yield

$$\frac{dj_p}{d\Omega} \sim \cos^2\gamma \left|\sum_m c_m Y_{l,m}(\theta_{\vec{p}}, \varphi_{\vec{p}})\right|^2. \tag{20}$$

Now consider the four bonding configurations of an adsorbate with a bonding p orbital on the simple-cubic face of a crystal. The y-oriented bridge bond is given by $c_1 = c_{-1} = 1$, $\Phi_y \sim Y_{1,1} + Y_{1,-1} \sim i\sin\theta_{\vec{p}}\sin\varphi_{\vec{p}}$, the x-oriented bridge bond by $c_1 = -c_{-1} = 1$ and $\Phi_x \sim Y_{1,1} - Y_{1,-1} \sim \sin\theta_{\vec{p}}\cos\varphi_{\vec{p}}$, the fourfold configuration by $\Phi_4 \sim \Phi_x \pm \Phi_y \sim \sin\theta_{\vec{p}}\, e^{\pm i\varphi_{\vec{p}}}$, and the head-on site by $\Phi_z \sim Y_{1,0} \sim \cos\theta_{\vec{p}}$. These quantities are the angular dependences within the modulus squared in Eq. (4). In order to proceed, take the photon angle of incidence to be 45° and let the y-z plane be the plane of incidence. The polar angles for s-polarized photons are $\theta_{\epsilon_s} = \pi/2$, $\varphi_{\epsilon_s} = 0$ and for p-polarized photons $\theta_{\epsilon_p} = \pi/4, \varphi_{\epsilon_p} = \pi/2$. From the equation for $\cos\gamma$,

$$\cos\gamma_s = \sin\theta\cos\varphi, \tag{21a}$$

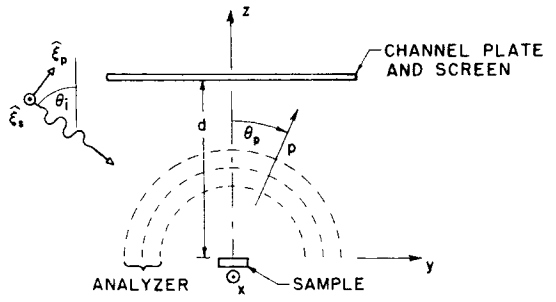

FIG. 3. Schematic picture of the photoemission angular-distribution visual display due to Plummer and Waclawski. The coordinate system, photon polarization vectors, and polar angles are shown.

$$\cos\gamma_p = (1/\sqrt{2})(\cos\theta + \sin\theta\sin\varphi), \tag{21b}$$

and for unpolarized light,

$$\cos^2\gamma_{un} = \tfrac{1}{2}(\cos^2\gamma_s + \cos^2\gamma_p). \tag{21c}$$

The complete AD's are given by combining Eqs. (20), (21), and the angular factors determined by the bonding wave functions.

Plummer and Waclawski[5,6] have designed an experiment in which a visual display of the photoemission AD can be observed and recorded. This is shown schematically in Fig. 3. Energy discrimination is accomplished by the three-grid retarding-potential analyzer. The electrons are accelerated to a channel-plate image intensifier and the multiplied current impinges on a flat fluorescent screen. Once the background or substrate emission is removed from the image (using either digital techniques or color superpositioning techniques of field ion microscopy[31]) the resulting pattern is a projection of the AD from the oriented atoms onto a flat screen.

The AD given by Eqs. (20) and (21) has been expressed in terms of Cartesian coordinates on the flat screen through $\sin\theta = (x^2+y^2)^{1/2}/(x^2+y^2+D^2)^{1/2}$, $\sin\varphi = y/(x^2+y^2+D^2)^{1/2}$, etc., with D the sample-to-screen separation. The measured quantity in the projection on the flat screen is the intensity per unit area ($\equiv dj/da$), which is related to the calculated AD through $dj/da = (\cos^3\theta/D^2)(dj/d\Omega)$. Contours of constant intensity have been drawn in the lower three rows of Fig. 4 for the four bond sites and three polarization states mentioned. The maximum-intensity contour usually is given as a dot. The difference between the maximum and minimum intensity is divided into ten equal increments. The contours are bounded by $|x|, |y| = 3D$.

It is to be noted that there is no simple one-to-one correspondence between the symmetry of the bond configuration and the symmetry of the emis-

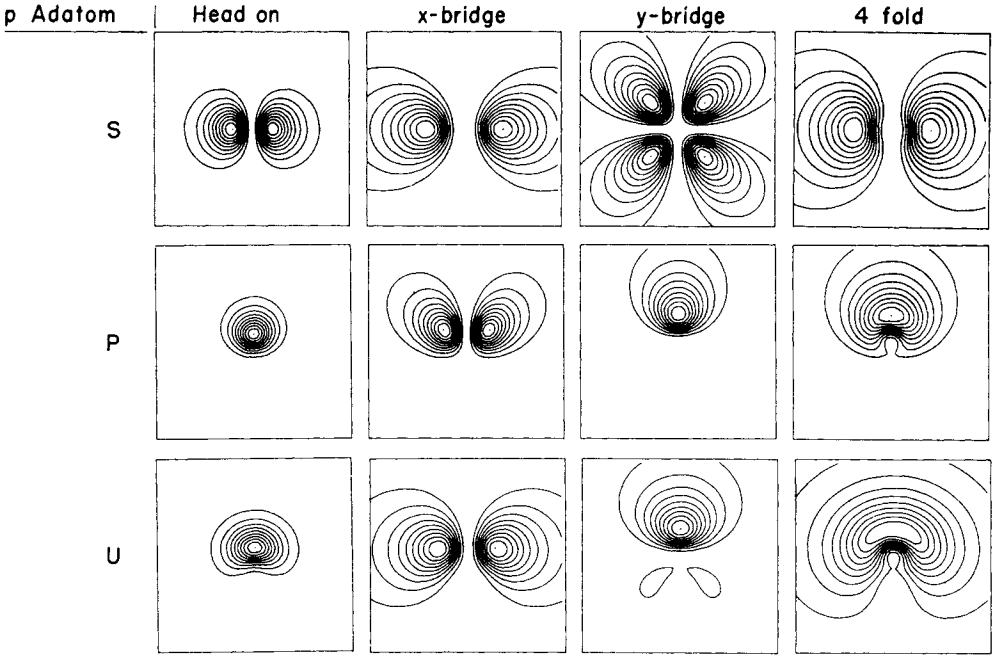

FIG. 4. Bond geometries and constant-intensity contours of photoemitted electrons from oriented p orbitals as projected on a screen parallel to the emitting surface. The incident angle of the photons is 45° and z-y plane is the plane of incidence. Bond geometries for the particular columns are labeled in the first row. The constant-intensity contours are shown in the remaining rows for s, p, and unpolarized photons, respectively. The maximum intensity is a factor of 10 larger than the minimum-intensity curved displayed. The interval between adjacent curves is $(I_{max}-I_{min})/10$. The curves are bounded by $|x_{max}|, |y_{max}| = 3D$.

TABLE I. Angular functions for the substrate d orbitals.

Label	Sum of $Y_{l,m}$	Function of angle
$d_{x^2-y^2}$	$(1/\sqrt{2})(Y_{2,2}+Y_{2,-2})$	$\frac{1}{2}(15/4\pi)^{1/2}\sin^2\theta\ (\cos^2\varphi-\sin^2\varphi)$
d_{xz}	$-(1/\sqrt{2})(Y_{2,1}-Y_{2,-1})$	$(15/4\pi)^{1/2}\sin\theta\cos\theta\cos\varphi$
d_{xy}	$(1/i\sqrt{2})(Y_{2,2}-Y_{2,-2})$	$(15/4\pi)^{1/2}\sin^2\theta\sin\varphi\cos\varphi$
d_{yz}	$(-1/i\sqrt{2})(Y_{2,1}+Y_{2,-1})$	$(15/4\pi)^{1/2}\sin\theta\cos\theta\sin\varphi$
d_{z^2}	$Y_{2,0}$	$\frac{1}{3}\sqrt{3}(15/4\pi)^{1/2}(\frac{3}{2}\cos^2\theta-\frac{1}{2})$

sion pattern. The important point is that for each bond configuration, there is a distinctly different pattern for a given polarization state and certainly it would be possible to ascertain the bonding geometry by correctly analyzing experimental data of this sort.

B. s adatom on d-band substrate

The importance of the substrate orbital symmetry and the bond-site structure factor are emphasized in the AD from a system of an s adatom on a d-band substrate. Since hydrogen chemisorption on transition metals has been a testing ground for both theoretical models and new experimental techniques the additional information from an AD would be useful, especially for determination of the bonding geometry.

The bond geometries to be considered are shown in Fig. 2. The adatom (which is taken to be hydrogen) and substrate momentum distributions are given, from Eq. (20), by $\varphi_{1s}(\vec{p})=f_{10}(p)Y_{00}(\theta,\varphi)$ and $\varphi_g(\vec{p})=f_{n2}(p)d_g(\theta,\varphi)$. Explicit expressions for the d_g's are given in Table I, where d is the atom-substrate separation. The bond-site structure factor, Eq. (19), has been evaluated for the geometry in Fig. 2 with both s and p adsorbates and the results are shown in Table II. Since $Y_{00}(\theta,\varphi)=1/(4\pi)^{1/2}$, Eq. (18) can be written

$$\frac{dj_a}{d\Omega}\sim\cos^2\gamma\left|1+r'\frac{d_g(\theta,\varphi)}{Y_{00}(\theta,\varphi)}S(s,g;\vec{p})\right|^2, \qquad (22a)$$

with

$$r'\equiv\frac{N_g\beta_g}{\epsilon_l-\bar{\epsilon}}\frac{f_{n2}(p)}{f_{10}(p)}\ . \qquad (22b)$$

Clearly the relative intensity of substrate to adsorbate emission is determined by the value of r'. To estimate r', the value of f_{n2}/f_{10}, which is a measure of the relative photoionization amplitudes from substrate to adsorbate, is required. Considering a W substrate in which $n=5$, this ratio has been calculated using both Slater and Herman-Skillman[32] W $5d$ wave functions. The results vary by an order of magnitude, depending on the particular approximate wave functions. Owing to this uncertainty, f_{52}/f_{10} will also be treated as a free parameter. Actually the AD given by Eq. (22a) has only one adjustable parameter, r' given by Eq. (22b), which is a combination of several unknowns. Typically $N_g\beta_g/(\epsilon_l-\bar{\epsilon})\approx 1$ so f_{52}/f_{10} determines r'. From the calculated values in the far-uv energy range, $0.25\lesssim f_{52}/f_{10}\lesssim 3$.

Plummer and Waclawski[6] and also Feuerbacher and Fitton[33] have observed structure in an ultraviolet-photoemission spectrum of H on (100) W ~10 eV below the vacuum level which is possibly a localized-surface-molecule level.[16] With 21.2-eV photons, the ejected-electron wave number is $p\sim 1.7$ Å^{-1}. In W, the lattice constant $a=3.16$ Å. In these calculations, $d=a/2$ will be assumed. Combining Eqs. (21) and (22), using the expressions for d_g and $S(s,g;\vec{p})$ given in Tables I and II, and using the parameters just mentioned, contours of constant emission intensity per area have been obtained for the same incident-light conditions used in Fig. 4. Contours in which $f_{52}/f_{10}=0.25$ are shown in Fig. 5 with $|x|, |y|\le 2D$, as is the case for all subsequent plots. Since emission from the H is so strong, the angular anisotropies due to $d_g(\theta,\varphi)$ and $S(s,g;\vec{p})$ are suppressed in these contours. Letting $f_{52}/f_{10}=3$, the calculated upper limit, the resulting set of contours is shown in Fig. 6. As is evident, angular anisotropies are much more dramatic, owing to the dominating influence of both d_g and S. The d-orbital symmetries are reflected in d_g. Owing to the different path lengths between each W atom in the surface molecule and the detector, the coherent emission from each of the N_g W atoms interferes, producing the angular anisotropies accounted for in $S(s,g;\vec{p})$. For $p=1.7$ Å^{-1}, differential path-length distances

TABLE II. Bond-site structure factors for s and p adsorbates on d-band substrates.

Bond site	g	$S(s,g;\vec{p})$	$S(p,g;\vec{p})$
(i) Head on	z^2	$e^{ip_z d}$	$-e^{ip_z d}$
(ii) Flat bridge $\begin{Bmatrix}x\\y\end{Bmatrix}$	x^2-y^2	$\pm\cos(p_{x,y}a/2)$	$\mp i\sin(p_{x,y}a/2)$
(iii) Out-of-plane bridge $\begin{Bmatrix}x\\y\end{Bmatrix}$	$\begin{Bmatrix}xz\\yz\end{Bmatrix}$	$ie^{ip_z d}(\sin p_{x,y}a/2)$	$-e^{ip_z d}\cos(p_{x,y}a/2)$
(iv) Flat fourfold	xy	$-\sin(p_x a/2)\sin(p_y a/2)$	$-i\cos(p_{x,y}a/2)\sin(p_{y,x}a/2)$

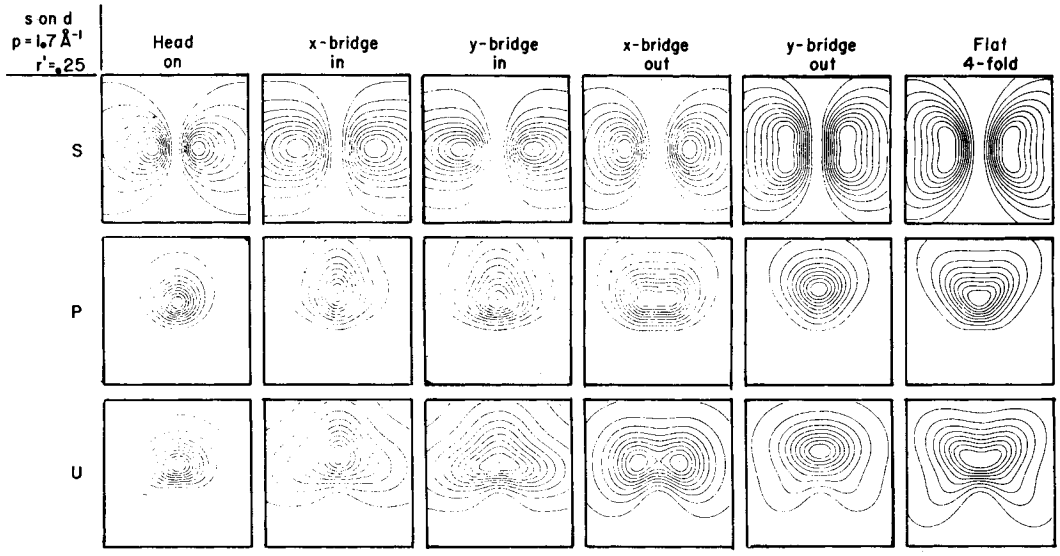

FIG. 5. Constant-intensity curves for an s atom on d-band substrate. The bond geometry and polarization state are labeled. The photon state is the same as in Fig. 4. The value of $\epsilon_I = -10$ eV with respect to the vacuum so for $h\nu = 21.2$ eV, $p = 1.7$ Å^{-1}. The parameter $r' = 0.25$. These curves and all remaining ones are bounded by $|x_{max}|, |y_{max}| = 2D$.

of the order of $\frac{1}{2}$ the electron wavelength occur only at larger θ where dj/da is reduced by the $\cos^3\theta$ geometrical factor. In Fig. 7, several sets of contours are shown for emission from the fourfold bond site using unpolarized light. The energy of the ejected electron is treated parametrically and it is assumed that $r' \gg 1$. As ϵ_f and thus p increase, the interference effects described by $S(s, g; \vec{p})$ become more important at smaller θ, nearer to the center of the screen, as is evidenced in Fig. 7. It would seem possible to separate the angular anisotropies due to orbital symmetries in d_g from the surface-molecule geometry in S, by measuring and analyzing the AD as a function of photon frequency. Indeed there is a wealth of information concerning surface-molecule structure in such data which should be accessible if the data are carefully analyzed.

C. p adatom on d-band substrate

The case of an adatom with a p valence shell adsorbed on a d-band substrate is particularly rele-

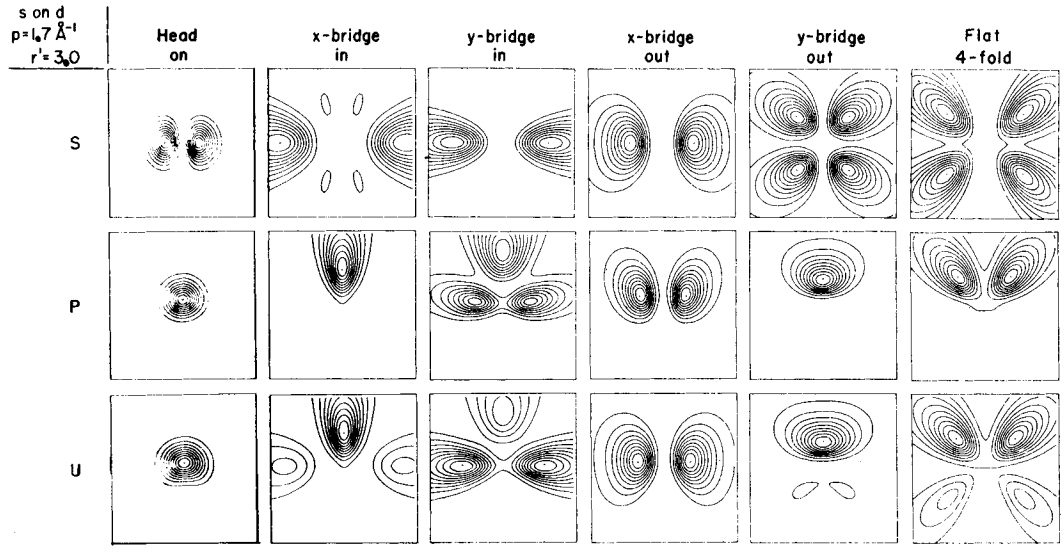

FIG. 6. Same as Fig. 5 but with $r' = 3$.

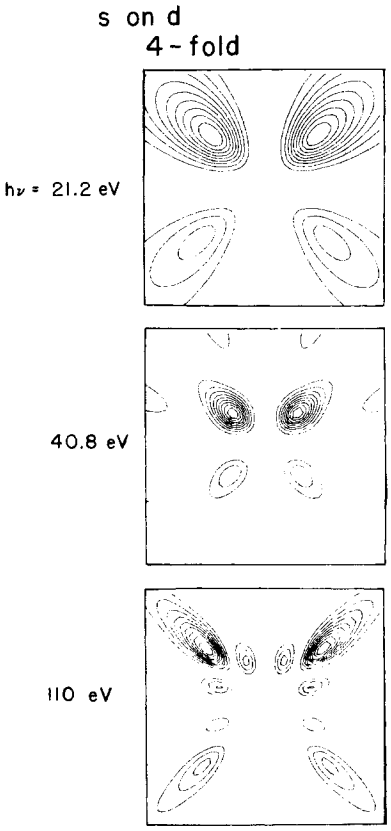

FIG. 7. Constant-intensity contours for emission from an s adatom in the flat fourfold site of a d-band substrate. In these curves $r' \gg 1$. With $\epsilon_l = -10$ eV, the photon energy is treated parametrically with $h\nu = 21.2$, 40.6, and 110 eV as labeled.

vant since chemisorptions of either O or C on transition metals are some of the most important and studied systems.

Again we will let the adatom adsorb in the six sites considered in Sec. V B. The normalized angular portions of the p orbitals are given in Table III. The bond-site structure factors, for p adsorbates, $S(p,g;\vec{p})$ are given in Table II. Special attention will be focused on the flat fourfold configuration shortly. As shown in Appendix B, the Fourier transform of an $l=1$ wave function is $\varphi_{n,1,m}(\vec{p}) = -4\pi i\, Y_{1m}(\theta_{\vec{p}}, \varphi_{\vec{p}}) f_{np}(p)$, whereas the transform of an $l=2$ wave function is $\varphi_{n'2,m'}(\vec{p}) = -4\pi\, Y_{2m'}(\theta_{\vec{p}}, \varphi_{\vec{p}}) f_{n'd}(p)$, where n, n' are the principal quantum numbers. Consequently the expression for the p-d AD, obtained from Eqs. (18) and (19), is

$$\frac{dj_g}{d\Omega} \sim \cos^2\gamma \left| p_j(\theta,\varphi) - ir' d_g(\theta,\varphi) S(p_j, g; \vec{p}) \right|^2 , \quad (23)$$

with $r' = [N_g \beta_g / (\epsilon_l - \bar{\epsilon})][f_{5d}(p)/f_{2p}(p)]$ and the subscript j denoting x, y, or z. To be specific, we consider the $5d$ W orbitals and the $2p$ O orbitals.

TABLE III. Angular functions for adsorbate p orbitals.

Label	Sum of $Y_{l,m}$	Function of angle
p_x	$(1/\sqrt{2})[Y_{1,-1} - Y_{1,1}]$	$(\frac{3}{4\pi})^{1/2} \sin\theta \cos\varphi$
p_y	$(i/\sqrt{2})(Y_{1,1} + Y_{1,-1})$	$(\frac{3}{4\pi})^{1/2} \sin\theta \sin\varphi$
p_z	$Y_{1,0}$	$(\frac{3}{4\pi})^{1/2} \cos\theta$

The same uncertainties in calculating r' as in Sec. V B are still with us, so r' will be treated parametrically with $r' = 0.1$, 1.0, and 3.0. The photon angle of incidence is 45° and the plane of incidence is the y-z plane.

A degree of ambiguity arises when considering the fourfold bond site. In Fig. 8 two plausible orbital configurations for the p-shell adsorbate are shown. In Fig. 8(a) the orbitals are just $\psi_1 = p_x$ and $\psi_2 = p_y$. There is a definite bond-site structure factor associated with each of these orbitals. In Fig. 8(b) two new orthogonal orbitals $\psi_1' \sim p_x + e^{i\delta_1} p_y$ and $\psi_2' \sim p_x + e^{i\delta_2} p_y$ are constructed from linear combinations of p_x and p_y with δ_1 and δ_2 phase factors.

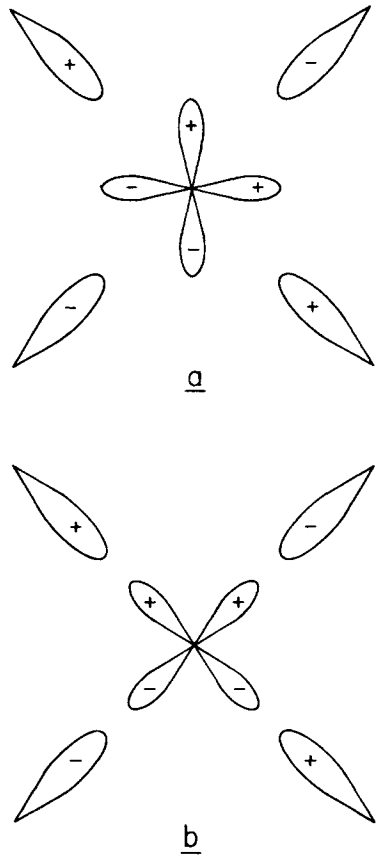

FIG. 8. Alternate, but equivalent, orbital configurations for a p-valence adatom in the flat fourfold site of a d-band metal.

No physical observable such as the AD can be a function of the arbitrary phases. Thus the AD from configuration (a) must be the same as that from (b). Furthermore the relative phase between ψ_1 and ψ_2 in Fig. 8(a) cannot be allowed to produce any physical consequence. The only scheme consistent with these requirements is one in which the emission from ψ_1 and ψ_2 or ψ_1' and ψ_2' adds incoherently. Thus the fourfold AD is

$$\frac{dj_{(a)-4}}{d\Omega} \sim \cos^2\gamma[|p_x - ir'd_{xy}S(p_x, xy; \vec{p})|^2 + |p_y - ir'd_{xy}S(p_y, xy; \vec{p})|^2], \quad (24)$$

where $S(p_x)$ and $S(p_y)$ are the two possibilites in the right-hand column, row four of Table II.

It is also worthwhile at this point to consider the theoretical distinction between a surface with uniform fourfold bond coordination and a surface with many domains of x- and y-oriented bridge bonds. As an example consider the expression for the AD from a surface with equal areas of x- and y-oriented flat-bridge-bond domains:

$$\frac{dj_{(a)-2}}{d\Omega} \sim \cos^2\gamma[|p_x - ir'd_{x^2-y^2}S(p_x, x^2-y^2; \vec{p})|^2 + |p_y - ir'd_{x^2-y^2}S(p_y, x^2-y^2; \vec{p})|^2]. \quad (25)$$

Owing to the different angular dependences between d_{xy} and $d_{x^2-y^2}$, and also between the different structure factors, Eqs. (24) and (25) are quite distinct and thus, in principle, an observation of the AD should allow one to differentiate between the fourfold bond and the degenerate x and y bridge bond. Only in the limit in which $r' = 0$, implicitly assumed in Sec. V A, would the two cases be indistinguishable.

In Figs. 9–11, contours of constant intensity per unit area, as projected on the fluorescent screen, have been drawn for the three polarization states and six bond geometries. As expected, the contours for small r', those in which emission from the p orbital dominates, are very similar to the contours in Fig. 4 for emission from simple-oriented p orbitals. As r' increases, the angular anisotropies become much more striking because of the effects of both the adsorbate and substrate orbitals and the bond-site structure factor. Note that in these contours, as in the previous ones, the maximum intensity often occurs at the positions of the dots in the figures.

In order to check whether fourfold-versus-degenerate-twofold bonding can be differentiated in an AD measurement, constant-intensity contours obtained from Eqs. (24) and (25) [i.e., $dj/da \sim \cos^3\theta \times (dj/d\Omega)$] for the case of normal-incidence unpolarized light have been calculated and are shown in Fig. 12. The ejected-electron wave number is 1.7 Å^{-1} and r' is treated parametrically. It is apparent that distinctly different AD's result in the two cases, for a given value of r', and thus there should be no problem, in principle, of distinguishing between the two. Note that for normal-incidence light, $\cos\gamma = \sin\theta$. Thus the quantity $\sin^2\theta\cos^3\theta$ multiplies the bracketed terms in Eqs. (24) and (25). This prefactor is peaked when $\tan^2\theta = \frac{2}{3}$ or $\theta \simeq 39°$, which accounts, in part, for the radial location of the maxima in Fig. 12.

Finally consider the actual case of O chemisorbed on (100) W. In the gas phase, the p_x, p_y, and p_z orbitals are degenerate. Upon chemisorption, it would be expected that at least some of this degeneracy would be lifted. Consider first the possibility of bonding in the head-on position. In this case, a molecular orbital is formed from a combination of the O p_z and W $d_{3z^2-r^2}$ orbitals and the resulting bonding orbital would lie lower in energy than either the unperturbed p or d orbitals do. On the other hand, the p_x and p_y orbitals do not participate in the bond, to first order, and thus their energy levels would be higher than the bonding orbital which includes p_z. Alternatively, if the O chemisorbs in either a bridge or fourfold site which involves p_x and p_y but not p_z, then the threefold degenerate O level is again split, but in this case the lower-lying bonding level contains p_x and p_y whereas the higher level contains p_z. It would be expected that the splitting would be of order 1 eV, the order of the chemisorption energy.

Using the photoemission apparatus shown in Fig. 3, Waclawski, Vorburger, and Stein[34] have obtained some preliminary data on the photoemission AD from O on (100) W. First the energy distribution, with 21.2-eV photons, was observed and two levels at ~ -5.8 and -7.0 eV with respect to the Fermi level were noted when O was chemisorbed. The lower level is interpreted here to be a bonding-surface molecular orbital and the higher one to be basically the remaining O orbital(s) not involved in the bond. Next, using phase-sensitive detection and a scanning-spot photometer, the differences between the AD with and without O, in the energy ranges $-5.8 \pm \sim 0.3$ eV and $-7 \pm \sim 0.3$ eV were obtained. The AD from the -5.8-eV level had a central maximum and no other significant structure characteristic of a p_z orbital. The lower level at -7 eV did have local maxima on either side of the plane of incidence, which is consistent with bridge or fourfold bonding. Owing to a number of technical problems in the experiment, a more quantitative analysis of the preliminary data would not be meaningful at this time. Among the problems are electron-optics effects which influence the θ dependence of the trajectories and a nonuniform gain across the channel-plate multiplier. In spite of these problems, it is encouraging to see that the AD technique can be implemented to provide bond-

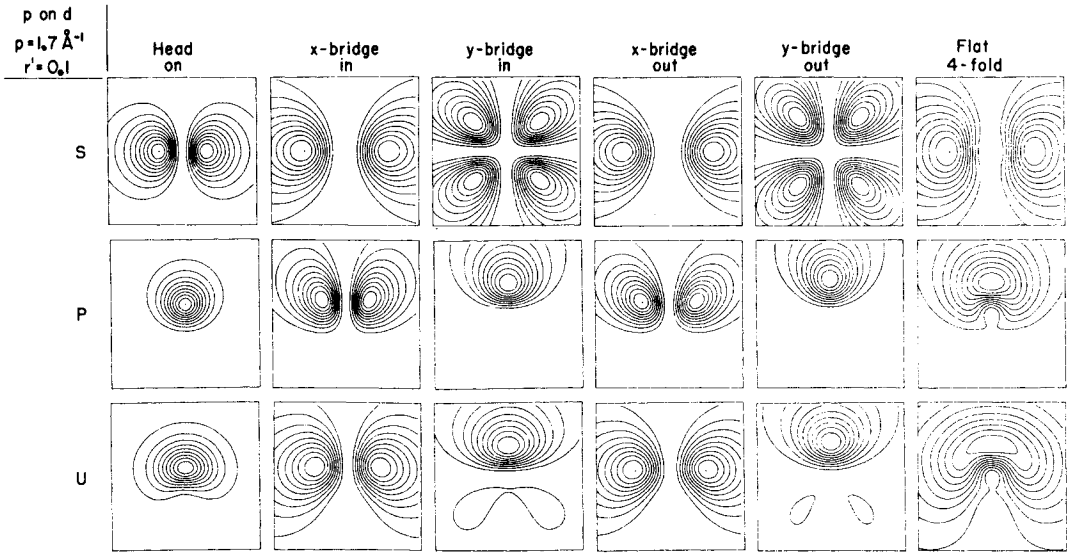

FIG. 9. Constant-intensity contours for a p adatom on a d-band substrate. The bond geometry and polarization state are labeled. The photon state is the same as in Fig. 4. The value of $\epsilon_f = -10$ eV with respect to the vacuum so for $h\nu = 21.2$ eV, $p = 1.7$ Å^{-1}. The parameter $r' = 0.1$.

geometry information. Small as this first specific conclusion is, that O on (100) W bonds is either in the bridge or fourfold site but not the head-on one, there is every reason to believe that future improvements in measurement systems will produce more quantitative information pertaining to bond geometry.

Since the submission of this manuscript, Traum and co-workers[35(a)] have observed photoemission AD's from the layered compound $TaSe_2$, which can roughly be regarded as a two-dimensional layer similar to a chemisorbed film. Their results offer encouragement that measurements of the type proposed here will provide useful structural information.

VI. CONCLUSIONS

A theory has been presented which attempts to explain the characteristics of electrons which have been photoejected from surface-molecule states formed in chemisorption of gases on transition-metal surfaces. In particular, the theory of the angular distribution of the photoejected electrons has been emphasized and it has been demonstrated

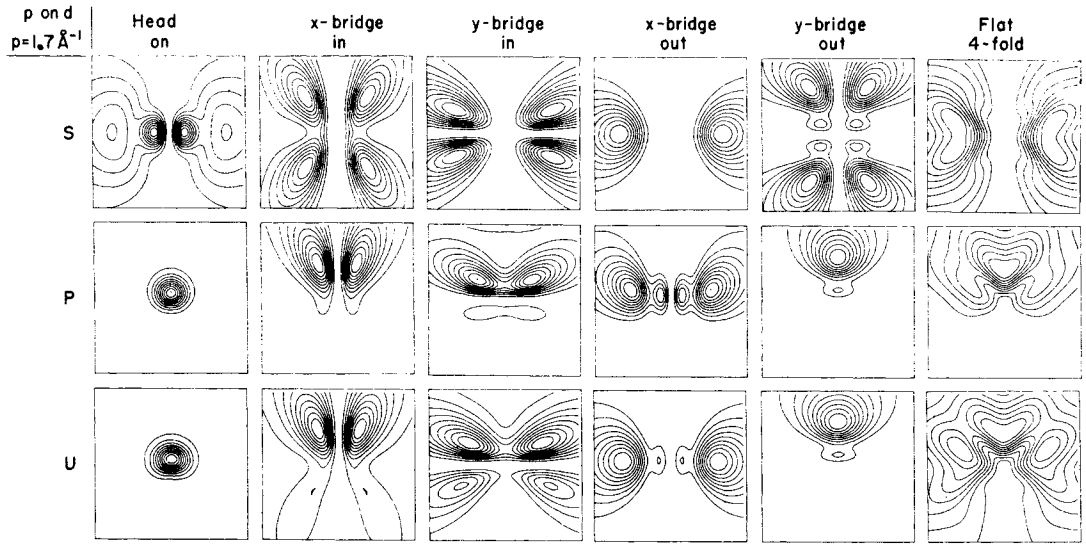

FIG. 10. Same as Fig. 9 but with $r' = 1.0$.

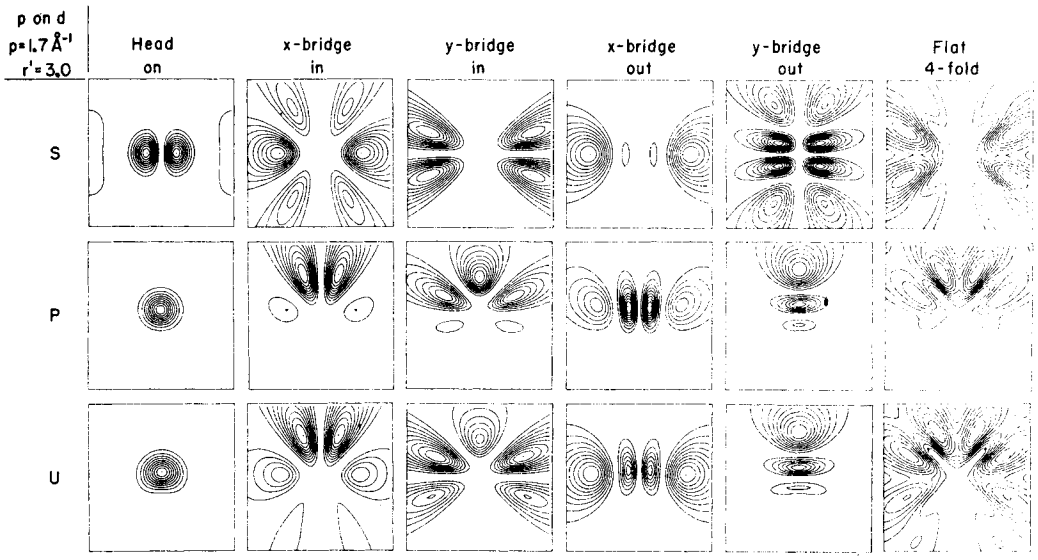

FIG. 11. Same as Fig. 9 but with $r' = 3.0$.

that the AD contains sufficient information to determine the chemisorption geometry. Numerous theoretical angular distributions have been presented for various combinations of adatom and substrate orbitals, bond geometries, photon energies, and the parameter r', which is a function of many unknown variables. In all cases, for set input parameters, photoemission from a surface molecule of a given bond geometry is distinctly different from that of any other geometry. There is the free parameter r' which cannot be specified from theoretical calculations more exactly than within an order-of-magnitude spread. However, it seems reasonable to follow the analytical procedure used by low-energy-electron-diffraction (LEED) theorists in analyzing data for determining bond geometries. That is, assume a particular geometry, calculate AD's for various values of r', and then repeat the procedure assuming a different geometry. This is ultimately repeated for all plausible geometries and values of r' and the geometry and value of r' which results in calculated curves agreeing best with the data is then declared the bonding geometry and experimentally determined value of r'. This operating procedure has allowed LEED theorists to make conclusions on chemisorption geometry[35-37] and there is no *a priori* reason why such a procedure should not be at least as applicable in photoemission AD analysis.

It appears that the presently suggested experiment is more straightforward than a LEED determination of the two-dimensional bond geometry for a fundamental reason. In LEED, the dominant angular effects are caused by coherent scattering from an array, and the angular dependence of the individual-atom scattering factor, which contains the presently desired information, is suppressed. On the other hand, in photoemission from submono-

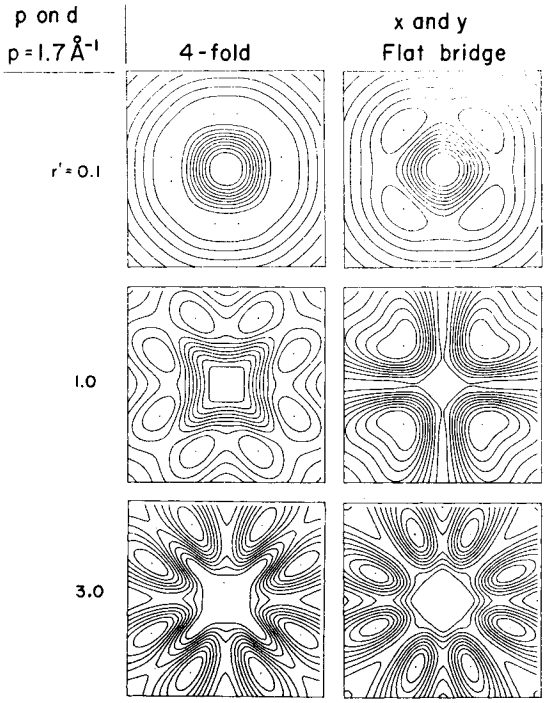

FIG. 12. Comparison between the constant-intensity contours from a p orbital in the flat fourfold site of a d-band substrate, the left column, and degenerate flat x and y bridge sites. Here unpolarized normal-incidence 21.2-eV light is used. With $\epsilon_f = -10$ eV, $p = 1.7$ Å^{-1}. The parameter $r' = 0.1$, 1.0, and 3.0.

layer films where two-dimensional band effects have yet to occur, the emission from a surface molecule is incoherent with respect to the emission from all other surface molecules and thus any angular effects reflect directly the angular dependence due to the individual atoms. For the same reasons, angular distributions of ions produced in electron-stimulated desorption are currently yielding rather unambiguous pictures of the bond geometry of individual chemisorbed atoms.[38]

Lastly, mention should be made of where to go from here. It would be desirable to repeat these calculations with a non-plane-wave final-state wave function. Aside from the excitonic final-state interactions, the plane-wave approximation should not be too severe, since the electrons which feel the surface and substrate periodic potential are those excited electrons which are directed into the solid and few of them will be elastically reflected back out towards the measuring apparatus.[21(b),21(c)] Another improvement would be to include more than first nearest neighbors in the surface molecule. Finally two-dimensional band effects between neighboring surface molecules could be treated. With this improvement, it would be a simple matter to adapt the formalism to a theory of bulk photoemission using a layer-upon-layer approach in a mixed $\vec{k}$ (transverse) and z (normal to surface) representation.[39]

ACKNOWLEDGMENT

The assistance of Dr. R. Celotta is gratefully acknowledged.

APPENDIX A

Throughout the text, it has been mentioned that one of the fundamental distinguishing features between atomiclike photoionization and solid-state photoemission is the degree of hole localization in the final state. In gas-phase photoionization, the hole is necessarily localized at one atomic center. Consequently, photoionization from each atom is an independent event, and thus there are no interference effects between photoionization amplitudes from each of the atoms in the ensemble. Even if the atoms were frozen into a crystalline array (with a very large lattice constant), if the hole remains localized, the photoionization from each atom adds incoherently and as a result, the conservation laws $\Delta l = \pm 1$, $\Delta m = 0, \pm 1$ arise. This has already been noticed by Mahan[7] in the case of x-ray photoemission from core states in solids. On the other hand if the hole delocalizes onto all atomic centers, as is usually implicitly assumed in solid-state photoemission, then the amplitudes for photoionization from each center add coherently and interference effects result. If the atoms are arranged in a crystalline array, the interference effects result in Bragg restrictions on the wave number of the final-state electron and thus conservation of $\vec{k}$ becomes meaningful. In either case, the dynamics of the hole determine the form of the final-state wave function, which in turn determines the importance of interference effects. Feynman[40] stated this effect (with specific reference to spin-flip–versus–non-spin-flip neutron scattering in magnetic materials) in terms of "records." If a probe such as the photon or neutron changes the internal state of one of the many possible scatterers and it is thus possible, in principle, to determine which scatterer or energy absorber was involved in a given event (due to spin flip in neutron scattering or localization of the hole in photoejection), then the amplitude for an event to occur at the center at $\vec{R}_i$ adds incoherently with the amplitude for the event to occur at each of the remaining centers. The fact that there is or is not a record of the event enters mathematically in our choice of final-state wave functions.

The preceding verbiage is easily illustrated explicitly for photoejection from a diatomic molecule of arbitrary internuclear separation, and the generalization to a many-center system (such as a solid) is straightforward. Consider an initial-state wave function of the Heitler-London form:

$$\psi_{\rm in} = (1/\sqrt{2})[\varphi_i(1)\varphi_j(2) \pm \varphi_i(2)\varphi_j(1)], \tag{A1}$$

where $\varphi_{i\,(j)}$ is the atomic orbital on center i (j) and 1, 2 are the coordinates of electron 1, 2. The Heitler-London form has the desirable characteristic that it gives the correct atomic behavior for the large internuclear separations experienced in the gas phase and is a reasonable approximation for small (~ atomic dimensions) separations. The two-electron–photon interaction is

$$\tau = (\hbar e/imc)\,\vec{A}\cdot(\vec{\nabla}_{\vec{r}_1} + \vec{\nabla}_{\vec{r}_2}). \tag{A2}$$

The final-state wave function falls into a domain bounded by two extremes. In the case of a localized hole, the photoejected electron originates from one center, say i, and the other electron remains on center j, at least for a time span which is long compared to the time in which the ejected electron is near the molecular ion, where there are strong final-state interactions. Consequently

$$\psi_{\rm fin} = (1/\sqrt{2})[\psi(1)\varphi_j(2) \pm \psi(2)\varphi_j(1)], \tag{A3a}$$

$$\psi_{\rm fin} = (1/\sqrt{2})[\psi(1)\varphi_i(2) \pm \psi(2)\varphi_i(1)]. \tag{A3b}$$

Combing Eqs. (A1) and (A3a), the optical matrix element is

$$u_{\rm loc} = \langle {\rm fin}\,|\,\tau\,|\,{\rm in}\rangle = (\hbar e/imc)\,\vec{A}\cdot\int d^3r\,\psi^*(\vec{r})\,\vec{\nabla}_{\vec{r}}\varphi_i(\vec{r}). \tag{A4}$$

If we make the further (but not essential) assumption that $\psi(\vec{r}) = e^{i\vec{B}\cdot\vec{r}}$, then since $\varphi_i(\vec{r}) = \varphi(\vec{r} - \vec{R}_i)$ with φ an atomic orbital with good angular mo-

mentum quantum numbers about $\vec{R}_i$, Eq. (4) becomes

$$u_{\rm loc} = (\hbar e/imc)\,(\vec{A}\cdot\vec{p})\,e^{-i\vec{p}\cdot\vec{R}_i}\varphi(\vec{p}) \tag{A5}$$

and

$$|u_{\rm loc}|^2 \sim \cos^2\gamma\,|\varphi(\vec{p})|^2,$$

independent of $\vec{R}_i$. This is the form of the gas-phase mod-squared matrix element since hole localization has been assumed.

The other extreme is complete hole delocalization, in which case (for a homonuclear molecule) the final-state wave functions are

$$\psi_{\rm fin} = \tfrac{1}{2}\psi(1)[\varphi_i(2)\pm\varphi_j(2)] \pm \tfrac{1}{2}\psi(2)[\varphi_i(1)\pm\varphi_j(1)], \tag{A6}$$

and the same with 1,2 reversed. Equation (A6) implies that the electron left behind on the molecule is shared between the two centers. Thus there is no record left concerning which center the ejected electron originated from. Combining Eqs. (A1), (A2), and (A6),

$$u_{\rm deloc} = (\hbar e/imc\sqrt{2})\,\vec{A}\cdot\int d^3r\,\psi^*(r)\vec{\nabla}_{\vec{r}}[\varphi_i(\vec{r})+\varphi_j(\vec{r})] \tag{A7}$$

or with $\psi = e^{i\vec{p}\cdot\vec{r}}$

$$u_{\rm deloc} = (\hbar e/imc\sqrt{2})\,(\vec{A}\cdot\vec{p})\varphi(\vec{p})\,(e^{-i\vec{p}\cdot\vec{R}_i}+e^{-i\vec{p}\cdot\vec{R}_j}).$$

The generalization of Eq. (A7) to N identical centers is straightforward and yields

$$u_{\rm deloc} = (\hbar e/imc\sqrt{N})\,(\vec{A}\cdot\vec{p})\,\varphi(\vec{p})\sum_i e^{-i\vec{p}\cdot\vec{R}_i},$$

which in the case of crystalline ordering becomes

$$|u_{\rm deloc}|^2 \sim \sum_G \cos^2\gamma\,|\varphi(\vec{p})|^2\,\delta^{(n)}(\vec{p}-\vec{G}), \tag{A8}$$

where n is the dimensionality of the array and $\vec{G}$ are the reciprocal-lattice vectors.

It can be argued that the Heitler-London initial-state overemphasizes correlations in the solid state and thus a molecular-orbital (for the diatomic molecule) or tight-binding Bloch function

$$\psi_{\rm in} = \frac{1}{\sqrt{N}}\sum_i e^{i\vec{k}\cdot\vec{R}_i}\,\varphi(\vec{r}-\vec{R}_i) \tag{A9}$$

is more appropriate, where $\vec{k}$ is the wave vector of the initial-band electron. Combining Eqs. (A2), (A6), and (A9) and using the same arguments leading to Eq. (A8), it is easy to show, for the crystalline array, that

$$|u_{\rm deloc}|^2 \sim \sum_G \cos^2\gamma\,|\varphi(\vec{p})|^2\,\delta^{(n)}(\vec{k}-\vec{p}-\vec{G}). \tag{A10}$$

In either Eq. (A8) or (A10), the momentum-conserving δ function, the "solid-state effect," is a result of the assumption of complete hole delocalization. From this discussion it has become apparent that both crystalline ordering and hole delocalization are necessary but not individually sufficient conditions for photoejection behavior usually associated with solid-state photoemission.

APPENDIX B

Here we consider the mathematical details of the Fourier transforms of atomic orbitals in fixed coordinate systems. The general atomic orbital is

$$\varphi(\vec{r}) = R_{nl}(r)\,Y_{lm}(\theta_r,\varphi_r) \tag{B1}$$

and the Fourier transform is

$$\varphi(\vec{p}) = \int d^3r\,e^{-i\vec{p}\cdot\vec{r}}\,\varphi(\vec{r}). \tag{B2}$$

The partial-wave expansion of the plane wave is

$$e^{-i\vec{p}\cdot\vec{r}} = 4\pi\sum_{l'=0}^{\infty}(-i)^{l'}j_{l'}(pr)\sum_{m'=-l'}^{+l'}Y_{l'm'}(\theta_p,\varphi_p)\times Y^*_{l'm'}(\theta_r,\varphi_r), \tag{B3}$$

where θ_p, φ_p are the angles of $\vec{p}$ and θ_r, φ_r the angles of $\vec{r}$ in the fixed coordinate system. Combining Eqs. (B1)–(B3),

$$\varphi(\vec{p}) = 4\pi(-i)^l Y_{lm}(\theta_p,\varphi_p)\int r^2 j_l(pr)R_{nl}(r)\,dr, \tag{B4}$$

which is just of the form $\varphi(\vec{p}) = f_{nl}(p)\,Y_{lm}(\theta_p,\varphi_p)$ given by Eq. (17). The important point is that $\varphi(\vec{p})$ possesses the same angular symmetry as $\varphi(\vec{r})$. For the cases considered in this paper,

$$\varphi_{l=0}(\vec{p}) = 4\pi\,Y_{00}(\theta_p,\varphi_p)\int r^2 j_0(pr)R_{10}(r)\,dr, \tag{B5a}$$

$$\varphi_{l=1}(\vec{p}) = -4\pi i\,Y_{1m}(\theta_p,\varphi_p)\int r^2 j_1(pr)R_{n1}(r)\,dr, \tag{B5b}$$

$$\varphi_{l=2}(\vec{p}) = -4\pi\,Y_{2m}(\theta_p,\varphi_p)\int r^2 j_2(pr)R_{n2}(r)\,dr. \tag{B5c}$$

Podolsky and Pauling[30] have evaluated Eqs. (B5a)–(B5c) for hydrogenic wave functions. If instead Slater functions,

$$\varphi_{nlm}(\vec{r}) = N_n r^{n-1}e^{-\xi r}Y_{l,m}(\theta,\varphi),$$

are chosen for the atomic orbital, with $N_n = (2\xi)^{n+1/2}/((2n)!)^{1/2}$, then Eqs. (B5a)–(B5c) are easily evaluated as

$$\varphi_{l=0}(\vec{p}) = 4\pi\,Y_{00}(\theta_p,\varphi_p)N_1[4\xi^{5/2}/(p^2+\xi^2)^2], \tag{B6a}$$

$$\varphi_{n=2,\,l=1}(\vec{p}) = -4\pi i\,Y_{1m}(\theta_p,\varphi_p)\,N_2\left(\frac{4\xi^{5/2}}{\sqrt{3}}\frac{1}{(p^2+\xi^2)^2}\times\left\{\frac{\xi}{p}-3\cos\left[4\sin^{-1}\left(\frac{p}{(\xi^2+p^2)^{1/2}}\right)\right]\right\}\right), \tag{B6b}$$

$$\varphi_{n=5,\,l=2}(\vec{p}) = -4\pi Y_{2,m}(\theta_p, \varphi_p) N_5 \left(\frac{6}{p(p^2+\xi^2)^2} \times \left\{ \frac{3}{p^2} \sin\left[4\tan^{-1}\left(\frac{p}{\xi}\right)\right] - \frac{20}{(p^2+\xi^2)} \sin\left[6\tan^{-1}\left(\frac{p}{\xi}\right)\right] - \frac{12}{p(p^2+\xi^2)^{1/2}} \cos\left[5\tan^{-1}\left(\frac{p}{\xi}\right)\right] \right\}\right). \quad \text{(B6c)}$$

Equations (B6a)–(B6c) were used to obtain values of $f_{52}(p)/f_a(p)$ mentioned in the text. The Slater constant was determined by setting $\xi = n/\langle r\rangle$, where $\langle r\rangle$ is the radius of maximum charge density of the particular orbital. Unfortunately the Slater functions severely underestimate $\varphi_{52}(p)$ compared to Herman-Skillman functions since the Slater functions drop off approximately exponentially for $r > \langle r\rangle$. On the other hand, Herman-Skillman $5d$ functions drop off very slowly with r and may overestimate the charge density at large r. For $p = 1.7$ Å^{-1}, $j_2(pr)$ in Eq. (B5c) has its maximum value at $r \simeq 2.25$ Å, where the Slater function is a poor approximation due to its smallness in this region. In contrast, the Herman-Skillman function may be too large at this radius. For this reason we have used the Slater and Herman-Skillman matrix elements as lower and upper limits when assigning values to f_{52}/f_{nl} $(n = 1, 2,\ l = 0, 1)$.

[1] D. E. Eastman and J. K. Cashion, Phys. Rev. Lett. 27, 1520 (1971).

[2] B. J. Waclawski and E. W. Plummer, J. Vac. Sci. Technol. 10, 292 (1973).

[3] J. M. Baker and D. E. Eastman, J. Vac. Sci. Technol. 10, 223 (1973).

[4] D. E. Eastman and W. D. Grobman, Phys. Rev. Lett. 30, 177 (1973).

[5] E. W. Plummer and B. J. Waclawski, 33rd Physical Electronics Conference, Berkeley, Calif., 1973 (unpublished).

[6] E. W. Plummer, B. J. Waclawski, and T. V. Vorburger, Chem Phys. Lett. 28, 510 (1974).

[7] G. D. Mahan, Phys. Rev. Lett. 24, 1068 (1970); Phys. Rev. B 2, 4334 (1970).

[8] U. Gerhardt and E. Dietz, Phys. Rev. Lett. 26, 1477 (1971).

[9] T. Gustafsson, P. O. Nilsson, and L. Wallden, Phys. Lett. A 27, 121 (1971).

[10] (a) R. Y. Koyama and L. R. Hughey, Phys. Rev. Lett. 29, 1518 (1972); (b) N. V. Smith and M. M. Traum, Phys. Rev. Lett. 31, 1247 (1973).

[11] J. W. Gadzuk, 32nd Physical Electronics Conference, Albuquerque, N. M., 1972 (unpublished); J. Vac. Sci. Technol. 11, 275 (1974); Solid State Commun. 15, 1011 (1974).

[12] T. B. Grimley, J. Vac. Sci. Technol. 8, 31 (1971).

[13] J. R. Schrieffer, J. Vac. Sci. Technol. 9, 561 (1972).

[14] B. J. Thorpe, Surf. Sci. 33, 306 (1972).

[15] D. R. Penn, Surf. Sci. 39, 333 (1973).

[16] J. W. Gadzuk, in *Surface Physics of Crystalline Materials*, edited by J. M. Blakely (Academic, New York, to be published); Surf. Sci. 43, 44 (1974).

[17] M. J. Kelly. Surf. Sci. 43, 587 (1974).

[18] J. Cooper and R. N. Zare, J. Chem. Phys. 48, 942 (1968).

[19] S. T. Manson, Phys. Rev. Lett. 26, 219 (1971).

[20] D. J. Kennedy and S. T. Manson, Phys. Rev. A 5, 227 (1972).

[21] (a) D. Dill, Phys. Rev. A 6, 160 (1972). (b) A. Liebsch, Phys. Rev. Lett. 32, 1203 (1974). (c) However, for the choice of parameters used in the published work of Liebsch, the angular anisotropies are weaker than those presented here.

[22] (a) The vector potential $\vec{A}$ should be associated with the total field (external plus induced) at the location of the surface molecule. Whether this is adequately represented by the external or the internal $\vec{A}$ is not clear since the surface molecule is located within the transition region. Assuming that one solved the boundary-value problem correctly, $\vec{A}$ in the subsequent formulas should be regarded as the total vector potential. If this differs substantially from $\vec{A}_{\text{external}}$, then θ_i must be modified. For further discussion of this point see E. W. Plummer, 34th Physical Electronics Conference, Murray Hill, N. J., 1974 (unpublished); P. J. Feibelman (unpublished); and P. J. Feibelman and D. E. Eastman Phys. Rev. B (to be published). (b) D. M. Newns, Phys. Rev. 178, 1123 (1969).

[23] D. R. Penn, Phys. Rev. Lett. 28, 1041 (1972).

[24] W. L. Schaich and N. W. Ashcroft, Phys. Rev. B 3, 2452 (1971).

[25] T. B. Grimley and M. Torrini, J. Phys. C 6, 868 (1973).

[26] Note that in almost all work up to the present, δ has been chosen to make the sine function vanish at the layer position one lattice constant out from the surface. Although this is as good as any arbitrary choice, the choice still remains arbitrary.

[27] W. E. Spicer, Phys. Rev. 154, 385 (1967).

[28] S. Doniach, Phys. Rev. B 2, 3898 (1970).

[29] M. L. Goldberger and K. M. Watson, *Collision Theory* (Wiley, New York, 1964), p. 540.

[30] B. Podolsky and L. Pauling, Phys. Rev. 34, 109 (1929).

[31] E. W. Müller and T. T. Tsong, *Field Ion Microscopy: Principles and Applications* (American Elsevier, New York, 1969).

[32] F. Herman and S. Skillman, *Atomic Structure Calculations* (Prentice-Hall, Englewood Cliffs, N. J., 1963).

[33] B. Feuerbacker and B. Fitton, Phys. Rev. B 8, 4890 (1973).

[34] B. J. Waclawski, T. Vorburger, and R. I. Stein, J. Vac. Sci. Technol. (to be published).

[35] (a) M. M. Traum, N. V. Smith, and F. I. DiSalvo, Phys. Rev. Lett. 32, 1241 (1974). (b) S. Andersson and J. B. Pendry, J. Phys. C 5, L 141 (1972).

[36] J. E. Demuth, D. W. Jepsen, and P. M. Marcus, Phys. Rev. Lett. 31, 540 (1973).

[37] C. B. Duke, N. O. Lipari, G. E. Laramore, and J. B. Theeten, Solid State Commun. 13, 579 (1973).

[38] J. Czyzewski, T. E. Madey, and J. T. Yates, Jr., Phys. Rev. Lett. 32, 777 (1974).

[39] Since the completion of this work, J. W. Cooper has pointed out to me the paper by I. G. Kaplan and A. P.

Markin, Dokl. Akad. Nauk SSR 184, 66 (1969) [Sov. Phys.-Dokl. 14, 36 (1969)]. In this paper, photoionization AD's from oriented H_2 molecules are calculated and emphasis is also placed on the interference effects noted in the present paper.

[40]R. P. Feynman, R. B. Leighton, and M. Sands, *Quantum Mechanics*, Vol. III of *The Feyman Lectures on Physics* (Addison-Wesley, Reading, Mass., 1965).